Tracking Mesoscale Convective Systems that are Potential Candidates for Tropical Cyclogenesis

KELLY M. NÚÑEZ OCASIO, JENNI L. EVANS, AND GEORGE S. YOUNG

Department of Meteorology and Atmospheric Science, The Pennsylvania State University, University Park, Pennsylvania

(Manuscript received 15 March 2019, in final form 15 November 2019)

ABSTRACT

This study introduces the development of the Tracking Algorithm for Mesoscale Convective Systems (TAMS), an algorithm that allows for the identifying, tracking, classifying, and assigning of rainfall to mesoscale convective systems (MCSs). TAMS combines area-overlapping and projected-cloud-edge tracking techniques to maximize the probability of detecting the progression of a convective system through time, accounting for splits and mergers. The combination of projection on area overlapping is equivalent to setting the background flow in which MCSs are moving on. Sensitivity tests show that area-overlapping technique with no projection (thus, no background flow) underestimates the real propagation speed of MCSs over Africa. The MCS life cycles and propagation derived using TAMS are consistent with climatology. The rainfall assignment is also more reliable than with previous methods as it utilizes a combination of regridding through linear interpolation with high temporal and spatial resolution data. This makes possible the identification of extreme rainfall events associated with intense MCSs more effectively. TAMS will be utilized in future work to build an AEW–MCS dataset to study tropical cyclogenesis.

1. Introduction

a. Mesoscale convective systems current understanding

A mesoscale convective system (MCS) can be defined as a cumulonimbus cloud system that produces a contiguous precipitation area with a width of 100 km or more in at least one direction (e.g., Houze 2004). MCSs can be initiated by orographic uplift (e.g., Houze et al. 1990). Over Africa, the Jos Plateau, Guinea Highlands, Marrah (Darfur) Mountains, and Ethiopian Highlands (Fig. 1) initiate such convective systems (Laing and Fritsch 1993; Hamilton et al. 2017; Mohr and Thorncroft 2006). The MCSs size, area coverage, and life cycle have been well documented (Maddox 1980; Mapes and Houze 1993; Laing and Fritsch 1993; Machado et al. 1993; Mathon and Laurent 2001; Evans and Jaskiewicz 2001; Tsakraklides and Evans 2003; Laing et al. 2008).

MCSs often cause severe weather, with major rainfall events being of particular interest. Analyses by Evans and Jaskiewicz (2001) showed that MCSs living longer than 6 h can contribute 50% of total regional rainfall. In the Sahel region, Mathon and Laurent (2001) showed that 60% of total cloud cover is due to such long-lived convective systems, which play an essential role in the hydrological cycle. In a recent work, Maranan et al. (2019) studied the dynamical and thermodynamical processes by which an intense MCS in the Guinea Coast region caused one of the highest ever recorded daily rainfall amounts on 12 June 2016. Not only do MCSs cause extreme rainfall events but also, the interaction between mesoscale convection and large-scale atmospheric conditions can be of critical importance in weather and climate over Africa and Atlantic main development region (MDR). Key features linking MCSs and tropical cyclogenesis are the African easterly jet (AEJ) and the African easterly waves (AEWs).

The dynamics of the AEJ were first studied by Carlson (1969), Burpee (1974) and Reed et al. (1977). The dynamical feedback between convection and the AEJ were studied by Thorncroft and Blackburn (1999) who described two diabatically forced meridional circulations responsible for the maintenance of the jet: one north of the AEJ, associated with surface fluxes and dry convection of the Saharan heat low, and the other south of the AEJ, associated with deep moist convection in the intertropical convergence zone (ITCZ). With the northward shift of the AEJ over the summer, long-lived convection (i.e., MCSs) is observed to occur in the

Corresponding author: Jenni L. Evans, jle7@psu.edu

DOI: 10.1175/MWR-D-19-0070.1

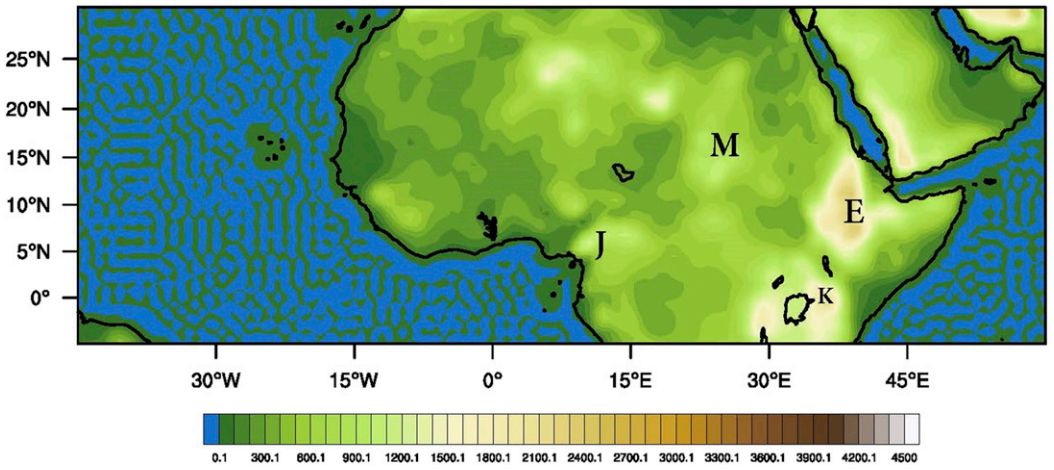

FIG. 1. Elevation map over domain in study using European Centre for Medium-Range Weather Forecasts (ECMWF) interim reanalysis (ERA-Interim) data. Labels were added to denote region of Marrah (Darfur) Mountains with the letter M, Ethiopian Highlands with the letter E, Jos Plateau with the letter J, and K for the region over Mount Kenya.

vicinity of the AEJ (e.g., Aspliden et al. 1976; Bolton 1984; Desbois et al. 1988; Rowell and Milford 1993; Hodges and Thorncroft 1997; Mathon and Laurent 2001). Intense convective systems over Africa follow the seasonal migration of the AEJ (Mohr and Thorncroft 2006). The hydrodynamic instability of the AEJ can initiate and maintain African easterly waves (AEWs) (Carlson 1969; Burpee 1974; Reed et al. 1977). Although in not all cases the MCS evolution is altered by AEWs, in some cases MCSs can move behind or ahead of an AEW trough in a nonlinear manner as they are coupled to the wave (Cifelli et al. 2010).

MCSs have also proven to have an important role in the initiation, growth and maintenance of AEWs. The first studies to show evidence that latent heat release also plays a significant role in the growth and maintenance of AEWs were Norquist et al. (1977) and Thorncroft and Hoskins (1994). The latter proposed AEWs to be Rossby waves (RWs) and undertook the analysis of these using potential vorticity (PV). Hsieh and Cook (2005) showed that MCSs can induce PV gradient reversals that can lead to initiation of AEWs. In addition, the coupling to convection has a large contribution to the synoptic PV (Berry and Thorncroft 2012). In an idealize modeling study Thorncroft et al. (2008) found that, after heating the region around Darfur (Marrah), AEWs can be generated by convection. In general, AEWs can form in response to convective events over Darfur (Marrah), develop baroclinically while being reinforced by diabatically generated PV and eventually undergo tropical cyclogenesis (Berry and Thorncroft 2005).

These studies have shown the undeniable role of convection (i.e., MCSs) in tropical cyclogenesis. A climatology of AEWs interaction with moist convection found that for composites of developing (undergo tropical cyclogenesis) and nondeveloping AEWs, that developing AEWs exhibited more convection and stronger low-level circulation, mainly over high mountains (Hopsch et al. 2010). Similarly, across AEW forecast ensemble members; developing members were more convectively active while crossing the coast compared to the nondeveloping members (Cecelski and Zhang 2013). These studies present evidence of the need to further understand the role of convection in AEWs growth and maintenance. In summary, MCSs play a significant role during the West African monsoon season, where the majority of the rainfall events are associated to them. In addition, MCSs have shown to have a key role on the initiation, maintenance and tropical cyclogenesis of AEWs. Because of their undeniable role in modulating the weather and climate over Africa and MDR, it is of importance to correctly identify, track, and classify MCSs. This study will focus on presenting a new method for identifying, tracking, classifying and assigning rainfall to MCS over Africa and to show its improved performance over previous methods. Next section will go over pioneering work on characterization and tracking of MCSs.

b. MCS satellite identification and tracking

Beginning in the 1980s, the identification and tracking of MCSs started to become more automated, using infrared (IR), or a combination of IR and visible images, to obtain characteristic temperatures and areas defining a cloud cluster (Velasco and Fritsch 1987; Augustine and Howard 1991; Laing and Fritsch 1993; Laing and Michael Fritsch 1997). Williams and Houze (1987) introduced the

area-overlapping technique for tracking individual cloud clusters through time using IR satellite data. Williams and Houze (1987) tracked clusters by first identifying individual cloud top areas with equivalent blackbody temperature less than 213 K to identify deep convection. If this area identified meets the size criterion of being sufficiently large (e.g., exceeding 5000 km^2), then it is deemed to be an MCS. To ascertain time continuity, overlap between consecutive satellite images is calculated. If overlap is at least 50%, the two features are judged to be the same MCS. The area-overlapping tracking technique has subsequently been used widely to track MCSs using IR imagery.

Evans and Shemo (1996) made use of the area-overlapping method and in addition, assigned rainfall to each system using two different IR-based rainfall algorithms. However, although the relative magnitude between systems were consistent for the two methods, there were quantitative differences in the rainfall diagnosed. Evans and Shemo (1996) tracking algorithm was improved by Tsakraklides and Evans (2003) where they included calculations of the complete set of system characteristics for warm cloud regions (235 K) as well as information on the growth in vertical, and horizontal extent of the system. Mathon and Laurent (2001) used an algorithm based on area overlap with an improvement of interpolating cluster life cycles in the case of missing data. Other methods, beyond area overlapping, have been developed and used in multiple studies.

Hodges (1995) developed a tracking technique that relies on minimization of a cost function to solve the correspondence problem and is defined in terms of local smoothness. These functions are constructed from local deviations of speed and direction of the MCS. The algorithm was improved to allow for missing satellite images using a checking method by tracking constraint of a smaller upper-bound displacement. The method showed some success as described in Hodges and Thorncroft (1997) and has been applied in multiple studies (e.g., Hopsch et al. 2010, 2007). However, the method also applied smoothing to the satellite data that may inhibit the detection of smaller convective systems. In addition, the method do not seem to assign rainfall to each MCS identified. Carvalho and Jones (2001) identified and tracked convective systems using the magnitudes of the spatial correlation between consecutive satellite images and the changes in horizontal areas of convective systems. Compared to Machado et al. (1998) which developed an automated overlapping method that assumes circular geometries for the systems overlapping and uses the weighted average of 28 structural properties, Carvalho and Jones (2001) method was an improvement as it allowed for diverse cloud shapes. Neither of these methods assigned rainfall to MCSs. Another major advance was the inclusion of propagation speed criterion by taking the area weighted centroid of the cloud in one satellite image and testing whether it is within a specified radial distance of the centroid in the previous satellite image (Woodley et al. 1980). Woodley et al. (1980) did assign rainfall to the MCSs. This approach was extended by a projected centroid location technique introduced by Johnson et al. (1998), where using the centroid locations from the previous volume scan radar data, a first guess at location for the current volume scan is generated. The first guess uses either the cell's previous motion vector or a default motion vector.

In recent years, Fiolleau and Roca (2013) developed a fully automated Tracking of Organized Convection (TOOCAN) algorithm for identification and tracking of MCSs. TOOCAN uses the most convective cores of the cloud top, identified by the lowest brightness temperature, and through clustering methods they associate the cloud clusters through time. TOOCAN enables the study of MCSs decomposed into their many small-scale features, which allows for an earlier detection in life cycle.

Whitehall et al. (2015) created a fully automated algorithm "Grab 'em Tag 'em, Graph 'em" (GTG) using graph theory. GTG identifies the cloud cluster with IR brightness temperature approach, creates a corresponding graph node, then using area overlap, the edges of the cloud cluster in consecutive satellite images are weighted according to percentage overlap. The algorithm also assigns rainfall using the Tropical Rainfall Measuring Mission (TRMM) 3-hourly product, 3B42 (Huffman et al. 2007). Application of GTG showed that the high overlapping percentage criterion (90%) in GTG makes the detection of small systems more difficult and inherently puts into question its ability to account for splits and mergers when small systems separate from bigger ones for example (e.g., Putri et al. 2017). In addition, the data are regridded to a coarser resolution.

All of these automated methods have furthered our understating of mesoscale convection and its importance in the different time scales. However, none of the past methods is able to effectively, identify, classify, track, and, assign rainfall to MCSs over Africa without showing some weakness either through methodology or by restricting resolution of satellite data ("smoothing"), which often times can limit the capacity of accounting for splits and mergers and the identification and tracking of smaller MCSs and/or cloud cluster associated to MCSs. To do this, a tracking algorithm should be able to account for the ever-moving background flow in which the MCSs are moving on that provides additional steering and thus, accelerate the systems. Thus, an algorithm that identifies,

tracks, classifies and assigns rainfall to MCSs throughout their entire lifespan, the Tracking Algorithm for Mesoscale Convective Systems (TAMS) has been developed. This two-step automated tracking algorithm is developed by combining the area-overlapping technique with a modified projection-cloud-edge technique. TAMS was developed with the goal to study MCSs that are coupled to AEWs to further understand their interaction and role in tropical cyclogenesis. However, the introduction and effectiveness of the algorithm is what will be presented in this work. After the validation of the algorithm, additional sections include an analysis of the life cycle evolution of MCS characteristics for systems in August and September of 2006. The next section describes data utilized and methodology.

2. Detection, tracking, classification, and rainfall assignment of MCSs with TAMS

a. Satellite data

Data from the Meteosat Second Generation (MSG) geostationary satellite, specifically the 10.8 μm spectral band of the Spinning Enhanced Visible and Infrared Imager (SEVIRI) imaging radiometer calibrated radiance, were used, where brightness temperature can be calculated by inverting the Planck function at the wavelength of the channel desired (Schmetz et al. 2002). This data were obtained at a 2-h intervals (although it can be obtained at higher temporal resolution) with a spatial resolution of 3 km. The domain selected extends over Africa and Atlantic Ocean, spanning latitudes from 5°S to 30°N and longitudes from 45°W to 60°E (shown on Fig. 1). The results presented are for the months of August–September 2006.

b. Identifying cloud elements (CEs)

Brightness temperature thresholds ranging between 253 K for the highest brightness temperature associated with convection to 213 K for very deep convection have been tested in the past for convective cloud detection (Maddox 1980; Duvel 1989, 1990; Machado et al. 1993; Mapes and Houze 1993; Mathon and Laurent 2001; Goyens et al. 2011). Machado et al. (1998) showed that the shape of the size distribution of the convective systems is not very sensitive to the choice of the temperature threshold (Mathon and Laurent 2001). Thus, selecting a temperature threshold between 213 and 253 K should allow the detection of convective systems. The 235 K threshold lies in the preferred range of temperature thresholds to capture the region of convection and accumulated rainfall (Evans and Jaskiewicz 2001; Tsakraklides and Evans 2003; Fiolleau and Roca 2013), and so is used here. If an area of 235 K or less brightness temperature also meets the condition of having an embedded region of 219 K area brightness temperature with an area $\geq$4000 km^2 (Tsakraklides and Evans 2003), then the 235 K area becomes a TAMS cloud element (CE), that is, a convective system candidate to be classified and tracked. In the following sections, the term cloud edge refers to the closed loop of pixels defining the CE.

Diagnostic variables are obtained from each CE to study the tracked system's characteristics and life cycle. These variables include the 2D centroid location (e.g., x and y components), area, and eccentricity (ε) of each CE at each IR observation time. Information on the growth in vertical, and horizontal extent of the system as described by Tsakraklides and Evans (2003) is also included (see below). The information for each CE is saved in a daily record that allows for the analysis of long-term datasets more efficiently. These daily structures are then the input used by TAMS to track, classify, and assign rainfall to each CE.

c. Tracking CEs

The tracking algorithm developed in this study is a combination of the area-overlapping technique (e.g., Williams and Houze 1987; Augustine and Howard 1991; Evans and Shemo 1996; Tsakraklides and Evans 2003; Machado et al. 1998; Mathon and Laurent 2001) and a modified version of the Lagrangian centroid projection technique (Hall 1992; Johnson et al. 1998). CEs of the current image (CEs_{t_i} where t is for time) are compared to all the CEs from the next two available images (e.g., $\text{CEs}_{t_{i+1}}$ and $\text{CEs}_{t_{i+2}}$) using a Lagrangian centroid projection technique. The technique works as follows: using the x component of the centroid location of CEs_{t_i}, the CEs_{t_i} are projected using a fixed climatological zonal propagation speed two hours into the future (i.e., time of the next satellite image). MCSs over Sahelian region propagate westward, with increased speed and lifetime for the most organized types (Mathon and Laurent 2001), thus it is reasonable to assume that the zonal propagation speed for MCSs over this region is larger than the meridional component of the propagation speed. Therefore, using a zonal propagation speed to project CEs_{t_i} in order to preselect those that will undergo the area-overlapping condition is a logical step (next section test the sensitivity of using different climatological zonal propagation speed). In this sense, the CEs_{t_i} projection through a zonal propagation speed assignment simplifies the task of the area-overlapping component of the algorithm (Hall 1992) by increasing the amount of overlap at longer time intervals. This advantage is important over Africa and the tropical

TABLE 1. Criteria used to categorize the four classes of convection.[a]

Organized systems	Disorganized systems
Mesoscale convective complex (MCC)	Disorganized long-lived (DLL)
Size: <219 K region has area ≥25 000 km^2 <235 K region has area ≥50 000 km^2 Duration: size definitions are met for ≥6 h Shape: $\varepsilon = \sqrt{1-(b^2/a^2)} \leq 0.7$	Temperature: <219 K Duration: sustains for ≥6 h No size or shape criterion
Convective cloud cluster (CCC)	Disorganized short-lived (DSL)
Size: <219 K region has area ≥25 000 km^2 Duration: size definitions are met for ≥6 h Shape: no shape criterion	Temperature: <219 K Duration: sustains for ≤3 h No size or shape criterion

[a] TCs are not included as the goal of TAMS is to detect the MCSs coupled to the AEW related to TCs.

North Atlantic because MCS propagation speeds there are sufficient to lead to large displacements between satellite images and thus to markedly decrease the overlap between satellite-derived CEs, leading to false negatives in area-overlapping-only matching algorithms. This high propagation speed results from both the advection of cloud systems by the AEJ and by shear-enhanced propagation of the MCS relative to the AEJ here in the way (Markowski and Richardson 2010) describe.

Next, the area overlap of the projected CEs$_{t_i}$ with CEs$_{t_{i+1}}$ and CEs$_{t_{i+2}}$ is calculated. Williams and Houze (1987) showed that the range for percentage area overlapping for CEs that are the same system, is between 50% and 66%. Thus, if the area overlap is ≥55% the CEs$_{t_{i+1}}$ and/or CEs$_{t_{i+2}}$ become "kids" of the CEs$_{t_i}$ and their indices are saved with CEs$_{t_i}$ who become their "parent." In the same way the indices of CEs$_{t_i}$ (the parents) are saved with the kids (CEs$_{t_{i+1}}$ and CEs$_{t_{i+2}}$).

After all of the CEs for all satellite images go through this step, all of the CEs having a parent/kid relationship are then grouped into a "family" (e.g., the track of a system) using a recursive graph-walking function. This parent/kid graph approach can capture any number of splits and mergers over the lifetime of an MCS: if at one time a system has more than one kid, this will count as a split, where as, if at one time a system has more than one parent, this will count as a merge. Thus, the number of splits and mergers can be quantified. This capability is one of the major advantages of TAMS.

The sensitivity of the algorithm to the zonal propagation speed used for projection (reflecting background flow) is tested and results are presented in section 3. In addition, comparison of the new area-overlapping and projected-cloud-edge combined TAMS technique with the area-overlapping technique alone is presented. Next section refers to TAMS using area-overlapping alone (e.g., with no projection) as equal to setting projection speed to 0 m s^{-1}. The classification and rainfall assignments methodology follows.

d. Classifying and assigning rainfall to MCSs

After an MCS is identified and tracked through time by TAMS, its complete trajectory is studied so that the entire track can be assigned to a single class. Table 1 shows the criteria for classifying MCSs used in TAMS. These criteria follow Maddox (1980), Evans and Shemo (1996), and Tsakraklides and Evans (2003). The classification has two main categories: organized and disorganized systems. Mesoscale convective complexes (MCCs) fall under the organized category and are the only classification with a shape criterion, $\varepsilon < 0.7$. Thus, MCCs are more symmetrically organized systems. Note that eccentricity (ε) is calculated by fitting an ellipse to the CE with $\varepsilon = 0$ corresponding to a circle. Systems having $\varepsilon \leq 0.7$ are more symmetric, while the systems with higher ε are more elongated.

The second category of organized systems, those too elliptical to pass the MCC shape criterion, are convective cloud clusters (CCCs). A new category is added as well: disorganized long-lived systems (DLL). The DLL category is for systems that do not meet the organized systems area criterion, but nonetheless last longer than 6 h.

To assign rainfall to each MCS, TAMS uses data from the Integrated Multisatellite Retrievals for GPM (IMERG) (Hong et al. 2004; Joyce and Xie 2011; Huffman et al. 2007; Rudolf and Schneider 2005). These data were recently released on June 2019 and updated on 16 August 2019 to include estimates back to June 2000 (Huffman et al. 2019). These IMERG precipitation estimates are gauge-calibrated microwave–IR retrievals. These precipitation estimates have a 0.1° × 0.1° spatial resolution and are available every 30 min.

TAMS regrids IMERG from its roughly 10 km grid to that of the Meteosat IR data (3 km) for compatibility with the CE data. This regridding was accomplished by

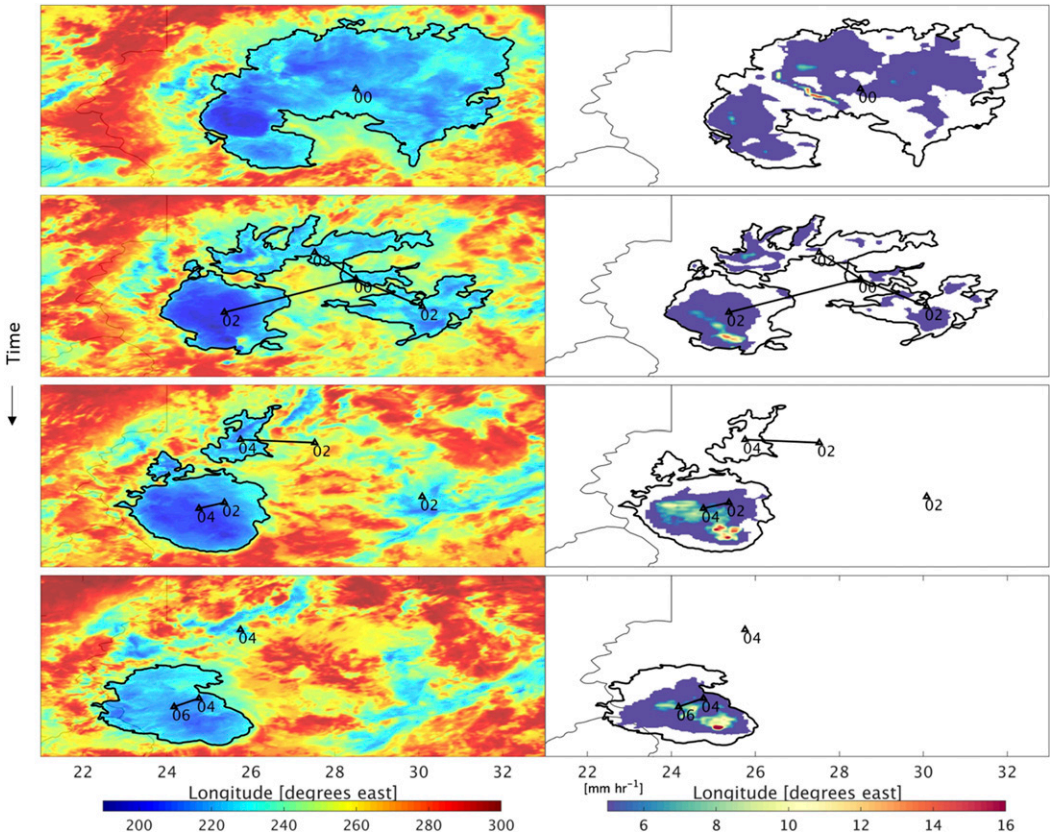

FIG. 2. (left) Brightness temperature satellite images with system centroid (or centroids) in black triangle with respective time and trajectory (black line) as identified and tracked by TAMS for a CCC. Note that the centroid and/or centroids of the previous image are included in the following to show the track evolution. (right) The respective rainfall assignment to each CE by TAMS.

linearly interpolating the IMERG estimates to the Meteosat grid. It should be noted that other interpolation methods were tested, including nearest neighbor, but the linear interpolation gave the best estimate. Precipitation for each CE for each time is then computed by summing over the CE. Total precipitation for each MCS is obtained by summing over all the CEs that are part of its family. The differences between MCS lifetime precipitation obtained using the different interpolation methods is fairly small. This is in keeping with previous findings where differences between interpolation methods were small at any one point, are smaller than the range in skill for a single method either across a domain, or in different seasons (e.g., Hofstra et al. 2008). Thus, using linear interpolation is appropriate.

Regridding from higher-resolution precipitation estimates such as IMERG rather than coarser TRMM 3B42 estimates, for example, is a significant TAMS improvement over other MCS tracking algorithms. Thus, the precipitation associated with different types of MCSs can be better to distinguish to further analyze its implication on MCS structure, evolution, and impact. Rossow et al. (2013) showed that higher-resolution data can capture extreme precipitation values more accurately. MCSs are the cause of extreme rainfall events as discussed in the introduction, and examples of those are the Nigerian intense MCS case on 12 June 2016 (Maranan et al. 2019) and the Ouagadougou case (Engel et al. 2017; Lafore et al. 2017).

Using high-resolution data together with an appropriate interpolating method enables accurate representation of precipitation associated to MCSs, better estimates of extreme rainfall events and better understating of the role of MCSs in tropical cyclogenesis. While all these are crucial for future applications of TAMS, this study focuses on introducing TAMS and validating its performance.

To illustrate all of this in practice, an example of how TAMS successfully identifies, tracks, classifies, and, assigns rainfall to a CCC is shown on Fig. 2. Note how between times 0000 and 0200 UTC the CCC experiences a split where 3 different CEs associated to this system separate from the cloud with the lowest brightness temperature (blue) and, thus, the most convective. By time

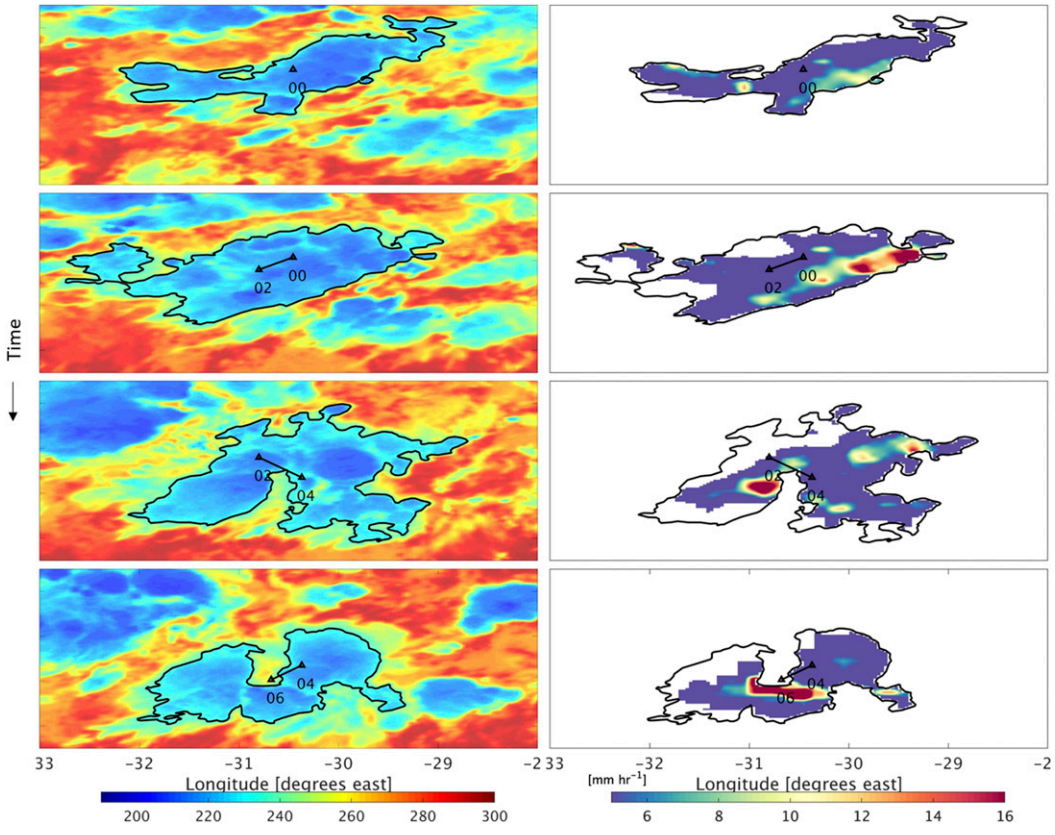

FIG. 3. As in Fig. 2, but for a DLL case.

0400 UTC the cloud with lowest brightness temperature has moved southwestward, one of the CEs (north of the most convective cloud) has moved westward and remains part of the CCC as identified by TAMS. The remaining two CEs have dissipated by this time. By 0600 UTC only the most convective of these CEs remains. TAMS successfully maintains track on each of the CEs until dissipation. The right-hand column of panels in Fig. 2 shows the corresponding rainfall assignment at each time and the corresponding cloud edge for each CE. Rainfall maxima are associated to the lowest brightness temperature areas corresponding with the more convective areas of the system. Figure 3 shows a corresponding example of the new DLL category. As described in Table 1, this type of MCS has no size or shape restrictions but must last at least 6 h. From the rainfall assignment is it is evident that is relevant to identify this type of system as they can produce copious amounts of rainfall.

Tracks for a sample of 25 MCSs identified, tracked, and classified by TAMS are shown in Fig. 4. These MCSs were active during the same time a developing AEW that then turn into Tropical Storm Debby was active. Note the nonlinearity of each of the tracks as MCSs cloud cluster split and merge throughout their lifetime. For example, the MCC track in light orange initiating around 37°E and 8°N starts propagating westward and turns northward as it approaches 30°E. Around 10.5°N a splitting occurs which is denoted by the smaller lines fanning out of the centroid. Later on, one of these CEs merge back into the parent system while the others dissipated. The system experiences one more split, near 22°E, with one CE moving south and dissipating and the other arcing to the north and west. This figure demonstrates that TAMS, by connecting the centroids of the parent systems and its associated CEs (kids), is able to track the complex trajectories of MCSs and their associated CEs. Next we explore the capability of TAMS combined technique not only to identify, track, classify and assign rain to MCSs over Africa, but also to reproduce propagation speeds consistent with known values for MCSs over Africa.

3. Validation of TAMS combined area-overlapping and projected-cloud-edge technique

a. Sensitivity of the MCSs propagation speeds to TAMS

To access the sensitivity of the TAMS combined area-overlapping and projected-cloud-edge technique to the

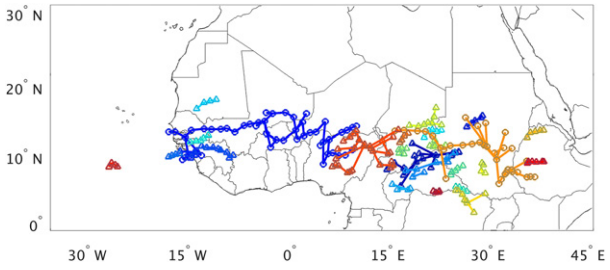

FIG. 4. 25 tracks of MCSs by TAMS from 17 to 21 Aug 2006 during the same time a developing AEW that then became Tropical Storm Debby was active. Triangles denote CCC's centroid position and circles MCC's centroid positions. The different colored tracks represent tracks of different MCSs.

assumed climatological propagation speed, four different zonal propagation speeds (5, 10, 12, and, 15 m s^{-1}) are tested to project the CEs as discussed in section 2c. In addition to these four sensitivity tests, an additional test is done using only the area-overlapping technique (and thus, 0 m s^{-1} as described in section 2c) to compare with the results of the proposed area-overlapping plus projected-cloud-edge technique. As described in section 2c, the reasoning behind combining area-overlapping with a projected-cloud-edge is to be able to account for the background flow in which MCSs move in. To test this idea, an analysis of the average propagation speeds obtained with each sensitivity test is done.

The average propagation speed is calculated for each MCS by taking the difference between its final and initial centroid position and dividing by its lifetime/duration. Normal kernel density estimations are used in this section to compute the distributions of average propagation speeds for MCSs and distributions of duration. This distribution fitting method is nonparametric in that it does not make any assumption about the shape of the underlying distribution, although it does require selection of the shape and bandwidth of the smoothing kernel (e.g., Hill 1985; Bowman and Azzalini 1997; Jones 1993). The bandwidth was optimized as in Bowman and Azzalini (1997). Nonparametric methods such as the kernel density distribution are more robust than parametric method because of the fewer assumptions made on the data and thus, it is used here to show data distribution as well as in the following section. Figure 5 shows the resulting distributions of average propagation speeds for MCCs, CCCs, and DLLs (refer to Table 1 for description MCS categories) tracked by TAMS. Several important observations can be made from the MCCs average propagation speed distributions (Fig. 5a). The first and most evident is that for all four sensitivity tests using projection (and thus accounting for background flow) the distributions modes lie between 10 and 13 m s^{-1}. Modes of the distributions for CCCs (Fig. 5b) lie in the same range with less of a spread in probability than MCCs. These results are suggesting that organized type convection over Africa propagate at a range of speeds that is consistent with previous work (e.g., Desbois et al. 1988; Barnes and Sieckman 1984; Laing et al. 2008; Mathon et al. 2002). An important outcome that supports the need to account for background flow is the low bias of the distribution of speeds for the area-overlap-only test (i.e., projection speed set to zero). This distribution is shifted to the left to the lower speed magnitudes and the mode lies at 7 m s^{-1} (Fig. 5a). This shift to the left for the area-overlap-only test is also seen for CCCs (Fig. 5b) and more evident for DLLs propagation speeds (Fig. 5c) which shows that the area-overlap-only test does not produce climatological values, in contrast to the TAMS combined technique.

An important result highlighted by these distributions is that the mode of the 12 m s^{-1} sensitivity tests lie beneath the value used for the projection, e.g., the 12 m s^{-1} projection sensitivity test highest probabilities lie close to 12 m s^{-1} and for the 10 m s^{-1} projection highest probabilities lie close to 10 m s^{-1}. Whereas the test using 5 and 15 m s^{-1} the peak does not lie at 5 and 15 m s^{-1} respectively but instead lies close to 10 and 12 m s^{-1}. Thus, even when the TAMS combined technique assumes a projection speed different from the previously observed climatological value of propagation speed, around 0–12 m s^{-1}, it yields propagation speed distribution closely matching those climatological values. In contrasts, the overlap-only methods yields a propagation speed distribution that is biased low by almost factor of two. Average background flow from the AEJ is typical between the range of 10 and 12 m s^{-1} which agrees well with these results (Burpee 1974; Cook 1999). These results show an additional application for TAMS as the projection (or background tuning) could be applied in future studies with other background flow settings.

Summarizing the results presented to this point it is proposed that TAMS can be used introspectively to select an appropriate zonal projection speed for its combined technique (background flow), and in that way is able to realistically represent propagation of MCSs over Africa (e.g., consistent with past literature). It is shown that the area-overlap-only method is not able to reproduce realistic propagation speed of MCSs, underestimating the propagation speed of MCSs. The distributions of the lifetime for each type of MCS in each sensitivity test is presented next.

b. *Sensitivity of the MCSs lifetimes to combined area-overlapping and projected-cloud-edge technique*

Figure 6 shows the lifetimes of MCSs obtained with the TAMS combined technique tests and the area-overlapping-only test. For CCC (Fig. 6b), lifetimes

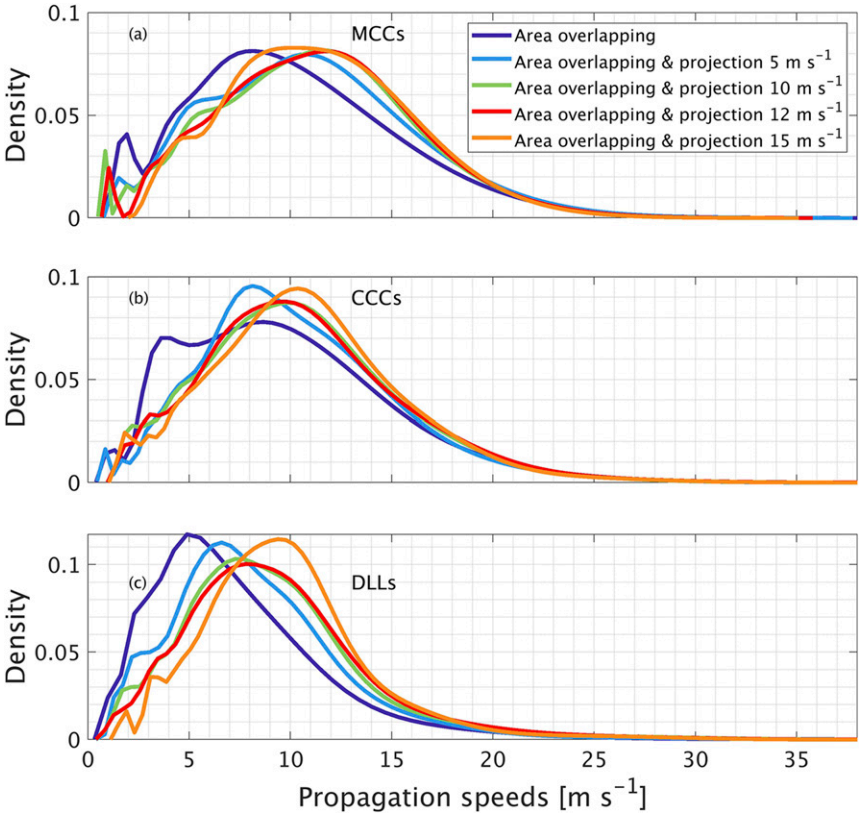

FIG. 5. Normal kernel density estimates of the distributions of average propagation speeds for (a) MCCs, (b) CCCs, and (c) DLLs using different zonal propagation speeds for projection tested in TAMS.

for all tests tend to correlate well with the mode of the distributions in 12 h. The correlation between tests is even more for DLLs where the mode of distributions is 6 h (Fig. 6c). For the MCCs (Fig. 6a) although the most probable lifetime is close to 12 h as in the CCCs case, the sensitivity tests differ on probability estimate, with the distribution acquiring a longer tail into long duration when a higher projection speed is assumed. This distribution asymptotes once the climatological propagation speed is reached. Thus, assuming a projection speed slower than the climatological propagation speed results in artificially truncated MCC lifetimes. This effect is most pronounced when the area-overlapping-only method is used. This suggest that the TAMS combined technique is able to more reliably capture longer-lived convection. This is relevant for TAMS applications as these longer-lived convective systems are potentially associated with developing AEWs and their eventual evolution into TCs. Thus, TAMS combined technique shows utility for AEW–MCS tropical cyclogenesis applications. These sensitivity results showed distinct differences on the propagation speed of MCSs (previous subsection) and the lifetime of MCCs over Africa, with the TAMS combined technique showing a better representation of the MCS propagation speeds and MCC lifetime than the area-overlapping-only technique.

c. *Sensitivity to splits and mergers of TAMS combined technique*

Splits and mergers of the IR cloud features complicate the task of MCS detection algorithms such as TAMS. Ideally, such a algorithm would, like TAMS, can keep track of the parent/kid relationship between system as they split and merge, so that the entire family could be treated as a whole. To test how well TAMS accomplishes this task, sensitivity studies were conducted. Table 2 shows ratio of splits to total number of systems (S_N), ratio of mergers to total number of systems (M_N), ratio of splits to total number of transitions times (S_t) and, ratio of mergers to total number of transition times (M_t) for each of the projection speed tests described above. It can be seen that the number of systems tracked and classified varies with the assumed projection speed, but stabilizes for any speed near the climatological value. Likewise, for both types of organized convection (i.e., MCCs and CCCs) TAMS combined technique is

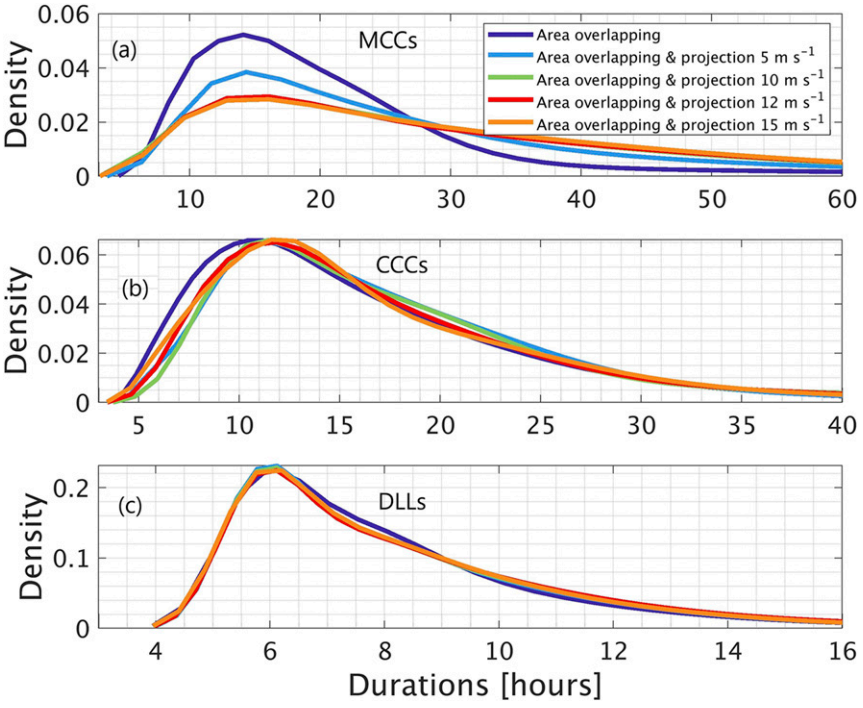

FIG. 6. Normal kernel distributions of lifetimes for (a) MCCs, (b) CCCs, and (c) DLLs using different zonal propagation speeds for projection tested in TAMS.

able to capture more splits and mergers when the assumed projection speed is near the climatological propagation speed. For DLLs, however, TAMS combined technique and area-overlapping-only technique have very similar results on split and merger statistics. Thus, use of a projection speed near climatology assists in monitoring splits and mergers, as well as the system propagation speed and lifetime as noted in previous sections.

The TAMS area-overlapping and projected-cloud-edge combined techniques also has the potential to help bridge

TABLE 2. Total number of systems (N), ratio of splits to total number of systems (S_N), ratio of mergers to total number of systems (M_N), ratio of splits to total number of transitions times (S_t), and, ratio of mergers to total number of transition times (M_t) for each of the projection speed tests.

			MCCs		
Projection speed	0 m s^{-1}	5 m s^{-1}	10 m s^{-1}	12 m s^{-1}	15 m s^{-1}
N	78	85	84	84	85
S_N	6.56	10.64	12.94	13.39	13.20
M_N	6.68	10.29	12.23	12.77	12.45
S_t	0.538	0.666	0.746	0.773	0.774
M_t	0.548	0.645	0.705	0.738	0.730
			CCCs		
N	207	195	182	186	180
S_N	4.41	5.26	6.12	5.94	5.78
M_N	4.41	5.19	5.91	5.71	5.67
S_t	0.491	0.547	0.609	0.613	0.608
M_t	0.4911	0.541	0.588	0.589	0.596
			DLLs		
N	357	432	409	396	361
S_N	1.23	1.19	1.48	1.54	1.62
M_N	1.28	1.30	1.60	1.65	1.71
S_t	0.243	0.232	0.290	0.301	0.323
M_t	0.253	0.253	0.313	0.323	0.342

over missing images. Hodges and Thorncroft (1997) tried to mitigate this issue for small gaps in the image series as discussed in section 1b. In TAMS this issue is mitigated by projecting system location to predict the approximate location of that system at the new, later, time. This propagation is equivalent to assuming a realistic background flow and system propagation relative to it. Doing so makes the task of the area-overlap component easier, particularly at longer image separation intervals as occur when a few images are missing from the series.

It should be mentioned that for the period in study (August through September 2006), the satellite data used has several instances where more than a few satellite images are missing, in the time window from 23 to 25 September. Even TAMS projection method cannot bridge these longer data gaps, so they will cut short the lifetime/duration of systems during that time period. This is noted in case of future studies application of TAMS during this time for this specific data. As long as analysis of MCSs focuses on characteristics of the different types of MCSs as a whole population and not the temporal evolution of cases (especially during the time of consecutive satellite images) it should not be an issue.

Being able to keep track of MCSs during splits and mergers means that TAMS can address the issue of complex trajectories as seen in Fig. 4 and detection of smaller CE features more accurately then the area-overlapping technique by itself. These smaller features are important for MCS morphology, evolution and MCS interaction with environmental features. Next section will analyze the evolution and characteristics of the MCSs identified in this study.

4. Life cycles and characteristics of organized convection for the August–September 2006

This section demonstrates the type of study that can be undertaken using TAMS.

a. Genesis and lysis of MCCs and CCCs

The following results are derived using TAMS combined technique of area-overlapping and cloud-edge projection/background flow of 12 m s^{-1}. Genesis and termination locations of MCC's centroids are plotted in Fig. 7c. The first observation is that there is a preferred region of genesis that lies to the east of 0° where most of the high mountain regions lie including the Marrah (Darfur), Ethiopian Highlands, and Kenya mountain region (see Fig. 1), although genesis can occur anywhere in that latitude band from Ethiopia west into the Atlantic. This preferred region of genesis is in agreement to past literature (e.g., Laing and Fritsch 1993; Hamilton et al. 2017). The presence of high terrain in both locations favors coherent convection by orographic uplift of warm air

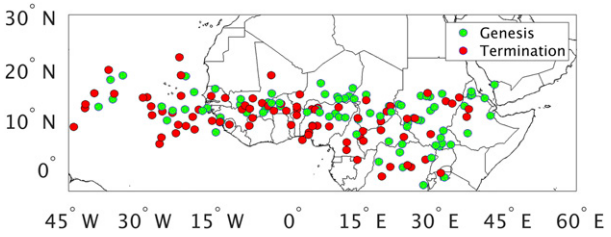

FIG. 7. Centroid genesis (green circles) and termination location (red circles) for MCCs for August through September 2006 over the region in study.

and by enhancing PV on the lee side of these mountains through vortex stretching from diabatic heating effects (Berry and Thorncroft 2005; Zehnder et al. 1999). Due to the westward propagation of these systems, the lysis occurrence lies to the west of genesis. Figure 8 shows that there are more CCC type of systems and that genesis and lysis are more broadly distributed across Africa and the Arabian Peninsula. Interestingly, genesis and lysis for CCCs are seen over the Yemen highland region where as it is not seen for MCCs. Likewise, closer to the equatorial belt there are more genesis and lysis occurrence for CCCs then for MCCs. Laing and Fritsch (1993) and Laing et al. (2011) showed that this region experiences the moderate low-level shear that is associated with the southwesterly monsoonal flow and midlevel easterly jets, they observed a lack of MCCs over the equatorial belt as well and agrees with these result. The morphology of organized convection is analyzed next.

b. Horizontal and vertical growth characteristics of MCCs and CCCs

The diurnal evolution of organized mesoscale convection (MCCs and CCCs) is discussed next (Figs. 9 and 10). For both CCCs (dashed lines) and MCCs (solid lines) categories, the preferred time of initiation is 1200–1400 UTC (Fig. 9a, green lines). Lysis/termination is most probable 0000–1000 UTC with MCCs showing a larger spread on the distribution of probable lysis times (solid dark orange line) suggesting longer lifetimes, which is consistent with previous studies (e.g., Maddox 1980; Laing and Fritsch 1993; Tsakraklides and Evans 2003).

Examination of the area evolution of CCCs (dashed violet line) and MCCs (solid violet line), shows a higher probability of systems obtaining maximum area extent 4–5 h after initiation between 1600 and 1900 UTC (Fig. 9b). As discussed above, (section 2, Table 1), eccentricity (ε) is calculated from the fitted ellipse of each CE, with $\varepsilon = 0$ corresponding to a circle. Systems having $\varepsilon \leq 0.7$ are more symmetric (and thus classified as MCC), while the systems with higher ε are more elongated. Turquoise lines in Fig. 9 indicate probability with

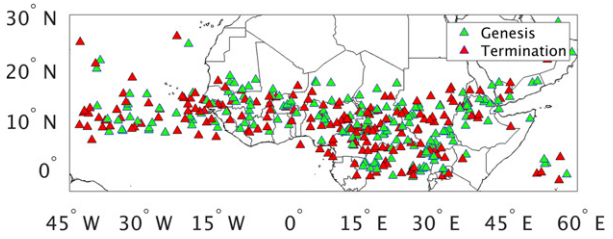

FIG. 8. Centroid genesis (green circles) and termination location (red circles) for CCCs for August–September 2006 over the region in study.

respect to time of systems attaining minimum ε, and thus, when mostly symmetric. Both CCCs and MCCs show most symmetry at the same time when maximum area extent is most likely, between 1600 and 1900 UTC. This correspondence between horizontal symmetry and maximum area extent is indicative of convective growth (Tsakraklides and Evans 2003). An interesting feature highlighted by these distributions is the second peak of likelihood of convective growth for both type of systems between 0300 and 0400 UTC during early morning hours when the radiative cooling effects at the top of the cloud are more pronounced.

To better understand the morphology of the systems tracked, the cold towers in the convective region (cloud top temperature less than 219 K) are examined. Low average cloud top temperatures suggest higher cloud top heights; similarly, high standard deviation of cloud top temperature suggest vertical overshoot above systems anvil (Tsakraklides and Evans 2003). Interestingly, the burst of convective towers as suggested by maximum standard deviation and minimum average cloud top temperature (Fig. 10a) is most probable at around 1–2 h prior to maximum area extent and symmetry is achieved. There is a hint of a second peak of likelihood of vertical overshoot consistent with the second peak of convective growth seen on Fig. 9b.

Consideration of rain rate (Fig. 10b) indicates an interaction between system area and cloud top structure: maximum area average rain rate is most probable close the most probable period of minimum average cloud top temperature and maximum standard deviation of the cold towers (Fig. 10a). These results are consistent with the rapid growth of an active convective system. Moreover, this peak in probability of maximum area average rain time is 1–2 h after initiation, although MCCs, do not show as pronounced a peak as CCCs, suggesting that MCCs have longer period of times of copious rainfall.

These results demonstrate that TAMS can be used to produce physically consistent multiparameter depictions of the life cycle of organized mesoscale convection. They are consistent with the evolution of organized convection as described by Houze (2004).

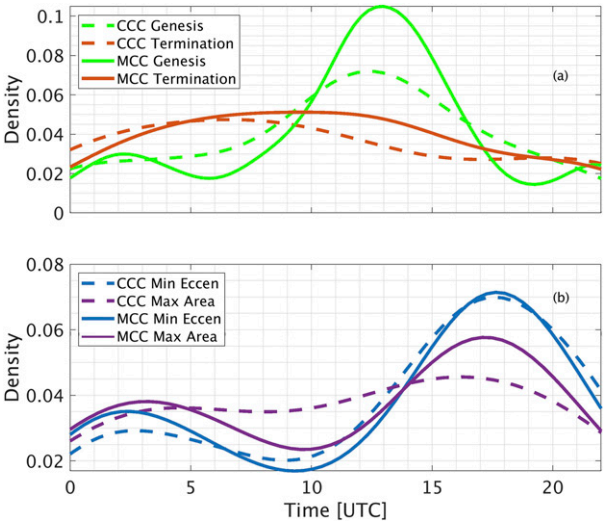

FIG. 9. Normal kernel density estimates of the distribution of diurnal variation of CCC (dashed) and MCC (solid) for (a) genesis (green) and termination (orange) and (b) maximum area (turquoise) and minimum eccentricity (purple, circular = 0). It is relevant to note for the interpretation of the following results that there are four different coordinated universal time (UTC) zones (UTC − 1, UTC, UTC + 1, UTC + 2) over the domain of Africa in study (5°S–30°N, 35°W–45°E). Although the domain in study is mostly under UTC and UTC + 1 time zones, objective analysis is done, thus times of day (morning, afternoon, night) are used as approximations with respect to the UTC time zone.

5. Discussion and conclusions

The Tracking Algorithm for Mesoscale Convective Systems (TAMS) combines the area-overlapping technique and a modified cloud-edge-projection technique, to efficiently track MCSs over Africa and the eastern Atlantic. The projection of cloud edges through the use of climatological MCS propagation speed, eases the task of the area-overlap method by increasing the likelihood of linking CEs that are part of the same system. This approach also makes it easier to account for splits and mergers. These results are proven to be relative insensitive to the projected speed as long as this value is close to the climatological MCS propagation speed of 12 m s^{-1}. In contrast, the area-overlapping method produces markedly different system statistics, including shorter lifetimes and propagation speeds which fall well below the climatological value. These improvements extend across MCS propagation speed, lifetime, and the likelihood of splitting and merger. Extension of this projection across the following two satellite images aids in mitigating the missing satellite data issue when there are only a few satellite images missing.

Area-overlapping technique if used by itself struggles to account for the splits and mergers of a system, potentially biasing downward the lifetimes of longer-lived

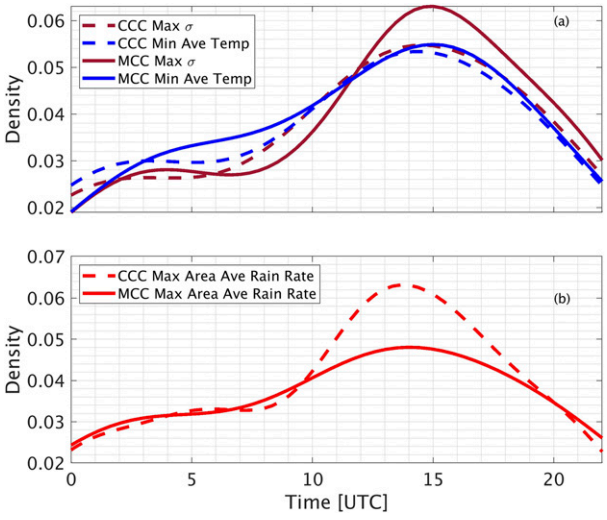

FIG. 10. As in Fig. 9, but for (a) minimum average temperature (blue) and maximum standard deviation (red) within cold cores and (b) maximum average rain rate (orange).

convection as seen from sensitivity tests, which shows that the area-overlapping-only technique (propagation speed of zero and thus, no background flow) resulted in a higher probability of shorter system lifetimes than any of the combined technique tests. TAMS shows skill in detecting correct propagation speeds of MCSs over Africa where as area overlapping by itself underestimates MCS propagation speed. Based on the sensitivity test using a projection between 10 and 12 m s^{-1} would be the correct projection to be utilized over Africa, an expected result because the AEJ mean wind speed lies close to these values. The background flow over Africa is extremely important as it is setting the stage for MCS propagation: the presence of the AEJ controls the mean wind for cell motion, and together with the AEJ, a very active southwesterly monsoon flow provides down shear propagation for the systems.

An additional feature of TAMS is its rainfall assignment that is more precise than previous methods because the regridding by linear interpolation is applied to new, high temporal and spatial resolution precipitation estimates (IMERG). This is important in MCS studies and further applications, as the usage of high-resolution estimates enables the possibility of accurately representing extreme rainfall events that over Africa can be associated to both intense MCS and MCS coupled to AEWs.

Results assuming a background flow of 12 m s^{-1} show that organized convection (both MCCs and CCCs) typical life cycle begins in the afternoon hours between 1200 and 1400 UTC with high convective activity obtaining maximum area extent and symmetry 4–5 h after initiation, terminating anywhere during 0000–1000 UTC as shown from the normal kernels distributions. Maximum area average rain rate for organized convection is most probable at around the most probable period of lowest average cloud top temperature and highest standard deviation of the cold towers, and thus, vertical overshoot.

The results presented here demonstrate that TAMS can characterize the life cycles and speeds of propagation of MCSs over Africa. Having a tool such as TAMS that not only is able to track both short- and long-lived convection, but can direct the user to the correct assignment of zonal propagation speed for projection could potentially help in the understanding of MCSs interaction with synoptic flow such as AEWs. Knowing the typical speeds of long-lived African MCSs can aid in the prediction of organized rainfall events.

Ongoing work with TAMS includes the application of TAMS to generate a composite of MCSs associated to developing versus nondeveloping AEWs to examine if interactions between the MCSs and AEW in an MCS–AEW couplet can be used to predict systems contributing to tropical cyclogenesis. This work may also be useful for assessing the potential for climate models to simulate tropical cyclogenesis.

Acknowledgments. We acknowledge the funding provided for this research from National Oceanic and Atmospheric Administration Educational Partnership Program under Agreement NA16SEC4810006-NCAS-M, and Penn State's African Research Center and Earth Environmental Systems Institute. Thanks to Penn State Institute of CyberScience for computer sources. Thank you to EUMETSAT for data access. Thanks to Dr. Jose Fuentes and Dr. Holly Hamilton for contributing knowledge on African climate and Dr. Kim Whitehall at Microsoft and Valencia College for guidance on tracking MCSs. We would also like to acknowledge Dr. Alan Brammer, University of Albany for providing AEW-TC tracks. Thank you to Chuck Pavloski for database management. Thank you to Zach Moon for guidance on database processing and analysis. We would also like to acknowledge Dr. Kelly Lombardo for contributing knowledge on MCS propagation.

REFERENCES

Aspliden, C. I., Y. Tourre, and J. B. Sabine, 1976: Some climatological aspects of West African disturbance lines during GATE. *Mon. Wea. Rev.*, **104**, 1029–1035, https://doi.org/10.1175/1520-0493(1976)104<1029:SCAOWA>2.0.CO;2.

Augustine, J. A., and K. W. Howard, 1991: Mesoscale convective complexes over the United States during 1986 and 1987. *Mon. Wea. Rev.*, **119**, 1575–1589, https://doi.org/10.1175/1520-0493(1991)119<1575:MCCOTU>2.0.CO;2.

Barnes, G. M., and K. Sieckman, 1984: The environment of fast- and slow-moving tropical mesoscale convective cloud

lines. *Mon. Wea. Rev.*, **112**, 1782–1794, https://doi.org/10.1175/1520-0493(1984)112<1782:TEOFAS>2.0.CO;2.

Berry, G. J., and C. Thorncroft, 2005: Case study of an intense African easterly wave. *Mon. Wea. Rev.*, **133**, 752–766, https://doi.org/10.1175/MWR2884.1.

——, and C. D. Thorncroft, 2012: African easterly wave dynamics in a mesoscale numerical model: The upscale role of convection. *J. Atmos. Sci.*, **69**, 1267–1283, https://doi.org/10.1175/JAS-D-11-099.1.

Bolton, D., 1984: Generation and propagation of African squall lines. *Quart. J. Roy. Meteor. Soc.*, **110**, 695–721, https://doi.org/10.1002/qj.49711046509.

Bowman, A., and A. Azzalini, 1997: *Applied Smoothing Techniques for Data Analysis: The Kernel Approach with S-Plus Illustrations.* Oxford University Press, 208 pp.

Burpee, R. W., 1974: Characteristics of North African easterly waves during the summers of 1968 and 1969. *J. Atmos. Sci.*, **31**, 1556–1570, https://doi.org/10.1175/1520-0469(1974)031<1556:CONAEW>2.0.CO;2.

Carlson, T. N., 1969: Some remarks on African disturbances and their progress over the tropical Atlantic. *Mon. Wea. Rev.*, **97**, 716–726, https://doi.org/10.1175/1520-0493(1969)097<0716:SROADA>2.3.CO;2.

Carvalho, L. M. V., and C. Jones, 2001: A satellite method to identify structural properties of mesoscale convective systems based on the maximum spatial correlation tracking technique (MASCOTTE). *J. Appl. Meteor.*, **40**, 1683–1701, https://doi.org/10.1175/1520-0450(2001)040<1683:ASMTIS>2.0.CO;2.

Cecelski, S. F., and D.-L. Zhang, 2013: Genesis of Hurricane Julia (2010) within an African easterly wave: Low-level vortices and upper-level warming. *J. Atmos. Sci.*, **70**, 3799–3817, https://doi.org/10.1175/JAS-D-13-043.1.

Cifelli, R., T. Lang, S. A. Rutledge, N. Guy, E. J. Zipser, J. Zawislak, and R. Holzworth, 2010: Characteristics of an African easterly wave observed during NAMMA. *J. Atmos. Sci.*, **67**, 3–25, https://doi.org/10.1175/2009JAS3141.1.

Cook, K. H., 1999: Generation of the African easterly jet and its role in determining West African precipitation. *J. Climate*, **12**, 1165–1184, https://doi.org/10.1175/1520-0442(1999)012<1165:GOTAEJ>2.0.CO;2.

Desbois, M., T. Kayiranga, B. Gnamien, S. Guessous, and L. Picon, 1988: Characterization of some elements of the Sahelian climate and their interannual variations for July 1983, 1984 and 1985 from the analysis of Meteosat ISCCP data. *J. Climate*, **1**, 867–904, https://doi.org/10.1175/1520-0442(1988)001<0867:COSEOT>2.0.CO;2.

Duvel, J. P., 1989: Convection over tropical Africa and the Atlantic Ocean during northern summer. Part I: Interannual and diurnal variations. *Mon. Wea. Rev.*, **117**, 2782–2799, https://doi.org/10.1175/1520-0493(1989)117<2782:COTAAT>2.0.CO;2.

——, 1990: Convection over tropical Africa and the Atlantic Ocean during northern summer. Part II: Modulation by easterly waves. *Mon. Wea. Rev.*, **118**, 1855–1868, https://doi.org/10.1175/1520-0493(1990)118<1855:COTAAT>2.0.CO;2.

Engel, T., A. H. Fink, and P. Knippertz, 2017: Extreme flooding in the West African cities of Dakar and Ouagadougou—Atmospheric dynamics and implications for flood risk assessments. *Proc. 19th EGU General Assembly (EGU2017),* Vienna, Austria, EGU, 11983.

Evans, J. L., and R. E. Shemo, 1996: A procedure for automated satellite-based identification and climatology development of various classes of organized convection. *J. Appl. Meteor.*, **35**, 638–652, https://doi.org/10.1175/1520-0450(1996)035<0638:APFASB>2.0.CO;2.

——, and F. A. Jaskiewicz, 2001: Satellite based monitoring of intraseasonal variations in tropical Pacific and Atlantic convection. *Geophys. Res. Lett.*, **28**, 1511–1514, https://doi.org/10.1029/1999GL011259.

Fiolleau, T., and R. Roca, 2013: An algorithm for the detection and tracking of tropical mesoscale convective systems using infrared images from geostationary satellite. *IEEE Trans. Geosci. Remote Sens.*, **51**, 4302–4315, https://doi.org/10.1109/TGRS.2012.2227762.

Goyens, C., D. Lauwaet, M. Schröder, M. Demuzere, and N. P. M. V. Lipzig, 2011: Tracking mesoscale convective systems in the Sahel: Relation between cloud parameters and precipitation. *Int. J. Climatol.*, **32**, 1921–1934, https://doi.org/10.1002/joc.2407.

Hall, D. L., 1992: *Mathematical Techniques in Multisensor Data Fusion*. Artech House, Inc., 320 pp.

Hamilton, H. L., G. S. Young, J. L. Evans, J. D. Fuentes, and K. M. N. Ocasio, 2017: The relationship between the Guinea Highlands and the West African offshore rainfall maximum. *Geophys. Res. Lett.*, **44**, 1158–1166, https://doi.org/10.1002/2016GL071170.

Hill, P., 1985: Kernel estimation of a distribution function. *Commun. Stat. - Theory Methods*, **14**, 605–620, https://doi.org/10.1080/03610928508828937.

Hodges, K. I., 1995: Feature tracking on the unit sphere. *Mon. Wea. Rev.*, **123**, 3458–3465, https://doi.org/10.1175/1520-0493(1995)123<3458:FTOTUS>2.0.CO;2.

——, and C. D. Thorncroft, 1997: Distribution and statistics of African mesoscale convective weather systems based on the ISCCP Meteosat imagery. *Mon. Wea. Rev.*, **125**, 2821–2837, https://doi.org/10.1175/1520-0493(1997)125<2821:DASOAM>2.0.CO;2.

Hofstra, N., M. Haylock, M. New, P. Jones, and C. Frei, 2008: Comparison of six methods for the interpolation of daily, European climate data. *J. Geophys. Res.*, **113**, D21110, https://doi.org/10.1029/2008JD010100.

Hong, Y., K.-L. Hsu, S. Sorooshian, and X. Gao, 2004: Precipitation estimation from remotely sensed imagery using an artificial neural network cloud classification system. *J. Appl. Meteor.*, **43**, 1834–1853, https://doi.org/10.1175/JAM2173.1.

Hopsch, S. B., C. D. Thorncroft, K. Hodges, and A. Aiyyer, 2007: West African storm tracks and their relationship to Atlantic tropical cyclones. *J. Climate*, **20**, 2468–2483, https://doi.org/10.1175/JCLI4139.1.

——, ——, and K. R. Tyle, 2010: Analysis of African easterly wave structures and their role in influencing tropical cyclogenesis. *Mon. Wea. Rev.*, **138**, 1399–1419, https://doi.org/10.1175/2009MWR2760.1.

Houze, R. A., 2004: Mesoscale convective systems. *Rev. Geophys.*, **42**, RG4003, https://doi.org/10.1029/2004RG000150.

——, B. F. Smull, and P. Dodge, 1990: Mesoscale organization of springtime rainstorms in Oklahoma. *Mon. Wea. Rev.*, **118**, 613–654, https://doi.org/10.1175/1520-0493(1990)118<0613:MOOSRI>2.0.CO;2.

Hsieh, J.-S., and K. H. Cook, 2005: Generation of African easterly wave disturbances: Relationship to the African easterly jet. *Mon. Wea. Rev.*, **133**, 1311–1327, https://doi.org/10.1175/MWR2916.1.

Huffman, G., and Coauthors, 2007: The TRMM Multisatellite Precipitation Analysis (TMPA): Quasi-global, multiyear, combined-sensor precipitation estimates at fine scales. *J. Hydrometeor.*, **8**, 38–55, https://doi.org/10.1175/JHM560.1.

——, E. Stocker, D. Bolvin, E. Nelkin, and T. Jackson, 2019: GPM_3IMERGHH: GPM IMERG final precipitation L3 half hourly 0.1 degree × 0.1 degree v06. Goddard Earth Sciences Data and Information Services Center (GES DISC), Greenbelt,

MD, accessed August–September 2019, https://doi.org/10.5067/GPM/IMERG/3B-HH/06.

Johnson, J. T., P. L. MacKeen, A. Witt, E. D. W. Mitchell, G. J. Stumpf, M. D. Eilts, and K. W. Thomas, 1998: The storm cell identification and tracking algorithm: An enhanced WSR-88D algorithm. *Wea. Forecasting*, **13**, 263–276, https://doi.org/10.1175/1520-0434(1998)013<0263:TSCIAT>2.0.CO;2.

Jones, C., 1993: Simple boundary correction for kernel density estimation. *Stat. Comput.*, **3**, 135–146, https://doi.org/10.1007/BF00147776.

Joyce, R. J., and P. Xie, 2011: Kalman filter–based CMORPH. *J. Hydrometeor.*, **12**, 1547–1563, https://doi.org/10.1175/JHM-D-11-022.1.

Lafore, J.-P., and Coauthors, 2017: A multi-scale analysis of the extreme rain event of Ouagadougou in 2009. *Quart. J. Roy. Meteor. Soc.*, **143**, 3094–3109, https://doi.org/10.1002/qj.3165.

Laing, A. G., and J. M. Fritsch, 1993: Mesoscale convective complexes in Africa. *Mon. Wea. Rev.*, **121**, 2254–2263, https://doi.org/10.1175/1520-0493(1993)121<2254:MCCIA>2.0.CO;2.

——, and ——, 1997: The global population of mesoscale convective complexes. *Quart. J. Roy. Meteor. Soc.*, **123**, 389–405, https://doi.org/10.1002/qj.49712353807.

——, R. Carbone, V. Levizzani, and J. Tuttle, 2008: The propagation and diurnal cycles of deep convection in northern tropical Africa. *Quart. J. Roy. Meteor. Soc.*, **134**, 93–109, https://doi.org/10.1002/qj.194.

——, R. E. Carbone, and V. Levizzani, 2011: Cycles and propagation of deep convection over equatorial Africa. *Mon. Wea. Rev.*, **139**, 2832–2853, https://doi.org/10.1175/2011MWR3500.1.

Machado, L. A. T., J.-P. Duvel, and M. Desbois, 1993: Diurnal variations and modulation by easterly waves of the size distribution of convective cloud clusters over West Africa and the Atlantic Ocean. *Mon. Wea. Rev.*, **121**, 37–49, https://doi.org/10.1175/1520-0493(1993)121<0037:DVAMBE>2.0.CO;2.

——, W. B. Rossow, R. L. Guedes, and A. W. Walker, 1998: Life cycle variations of mesoscale convective systems over the Americas. *Mon. Wea. Rev.*, **126**, 1630–1654, https://doi.org/10.1175/1520-0493(1998)126<1630:LCVOMC>2.0.CO;2.

Maddox, R. A., 1980: Meoscale convective complexes. *Bull. Amer. Meteor. Soc.*, **61**, 1374–1387, https://doi.org/10.1175/1520-0477(1980)061<1374:MCC>2.0.CO;2.

Mapes, B. E., and R. A. Houze, 1993: Cloud clusters and superclusters over the oceanic warm pool. *Mon. Wea. Rev.*, **121**, 1398–1416, https://doi.org/10.1175/1520-0493(1993)121<1398:CCASOT>2.0.CO;2.

Maranan, M., A. H. Fink, P. Knippertz, S. D. Francis, A. B. Akpo, G. Jegede, and C. Yorke, 2019: Interactions between convection and a moist vortex associated with an extreme rainfall event over southern West Africa. *Mon. Wea. Rev.*, **147**, 2309–2328, https://doi.org/10.1175/MWR-D-18-0396.1.

Markowski, P., and Y. Richardson, 2010: *Mesoscale Meteorology in Midlatitudes.* John Wiley and Sons, 430 pp., https://doi.org/10.1002/9780470682104.

Mathon, V., and H. Laurent, 2001: Life cycle of Sahelian mesoscale convective cloud systems. *Quart. J. Roy. Meteor. Soc.*, **127**, 377–406, https://doi.org/10.1002/qj.49712757208.

——, ——, and T. Lebel, 2002: Mesoscale convective system rainfall in the Sahel. *J. Appl. Meteor.*, **41**, 1081–1092, https://doi.org/10.1175/1520-0450(2002)041<1081:MCSRIT>2.0.CO;2.

Mohr, K. I., and C. D. Thorncroft, 2006: Intense convective systems in West Africa and their relationship to the African easterly jet. *Quart. J. Roy. Meteor. Soc.*, **132**, 163–176, https://doi.org/10.1256/qj.05.55.

Norquist, D. C., E. E. Recker, and R. J. Reed, 1977: The energetics of African wave disturbances as observed during phase III of GATE. *Mon. Wea. Rev.*, **105**, 334–342, https://doi.org/10.1175/1520-0493(1977)105<0334:TEOAWD>2.0.CO;2.

Putri, N. S., T. Hayasaka, and K. D. Whitehall, 2017: The properties of mesoscale convective systems in Indonesia detected using the grab 'em tag 'em graph 'em (GTG) algorithm. *J. Meteor. Soc. Japan*, **95**, 391–409, https://doi.org/10.2151/jmsj.2017-026.

Reed, R. J., D. C. Norquist, and E. E. Recker, 1977: The structure and properties of African wave disturbances as observed during phase III of GATE. *Mon. Wea. Rev.*, **105**, 317–333, https://doi.org/10.1175/1520-0493(1977)105<0317:TSAPOA>2.0.CO;2.

Rossow, W. B., A. Mekonnen, C. Pearl, and W. Goncalves, 2013: Tropical precipitation extremes. *J. Climate*, **26**, 1457–1466, https://doi.org/10.1175/JCLI-D-11-00725.1.

Rowell, D. P., and J. R. Milford, 1993: On the generation of African squall lines. *J. Climate*, **6**, 1181–1193, https://doi.org/10.1175/1520-0442(1993)006<1181:OTGOAS>2.0.CO;2.

Rudolf, B., and U. Schneider, 2005: Calculation of gridded precipitation data for the global land-surface using in-situ gauge observations. *Proc. Second Workshop of Int. Precipitation Working Group Workshop (IPWG),* Monterey, CA, EUMETSAT, 231–247.

Schmetz, J., P. Pili, S. Tjemkes, D. Just, J. Kerkmann, S. Rota, and A. Ratier, 2002: An introduction to Meteosat Second Generation (MSG). *Bull. Amer. Meteor. Soc.*, **83**, 977–992, https://doi.org/10.1175/1520-0477(2002)083<0977:AITMSG>2.3.CO;2.

Thorncroft, C. D., and B. J. Hoskins, 1994: An idealized study of African easterly waves. I: A linear view. *Quart. J. Roy. Meteor. Soc.*, **120**, 953–982, https://doi.org/10.1002/qj.49712051809.

——, and M. Blackburn, 1999: Maintenance of the African easterly jet. *Quart. J. Roy. Meteor. Soc.*, **125**, 763–786, https://doi.org/10.1002/QJ.49712555502.

——, N. M. J. Hall, and G. N. Kiladis, 2008: Three-dimensional structure and dynamics of African easterly waves. Part III: Genesis. *J. Atmos. Sci.*, **65**, 3596–3607, https://doi.org/10.1175/2008JAS2575.1.

Tsakraklides, G., and J. L. Evans, 2003: Global and regional diurnal variations of organized convection. *J. Climate*, **16**, 1562–1572, https://doi.org/10.1175/1520-0442-16.10.1562.

Velasco, I., and J. M. Fritsch, 1987: Mesoscale convective complexes in the Americas. *J. Geophys. Res.*, **92**, 9591–9613, https://doi.org/10.1029/JD092iD08p09591.

Whitehall, K., and Coauthors, 2015: Exploring a graph theory based algorithm for automated identification and characterization of large mesoscale convective systems in satellite datasets. *Earth Sci. Info.*, **8**, 663–675, https://doi.org/10.1007/S12145-014-0181-3.

Williams, M., and R. A. Houze, 1987: Satellite-observed characteristics of winter monsoon cloud clusters. *Mon. Wea. Rev.*, **115**, 505–519, https://doi.org/10.1175/1520-0493(1987)115<0505:SOCOWM>2.0.CO;2.

Woodley, W. L., C. G. Griffith, J. S. Griffin, and S. C. Stromatt, 1980: The inference of GATE convective rainfall from SMS-1 imagery. *J. Appl. Meteor.*, **19**, 388–408, https://doi.org/10.1175/1520-0450(1980)019<0388:TIOGCR>2.0.CO;2.

Zehnder, J. A., D. M. Powell, and D. L. Ropp, 1999: The interaction of easterly waves, orography, and the intertropical convergence zone in the genesis of eastern Pacific tropical cyclones. *Mon. Wea. Rev.*, **127**, 1566–1585, https://doi.org/10.1175/1520-0493(1999)127<1566:TIOEWO>2.0.CO;2.